Supplement of The Cryosphere, 19, 4373–4390, 2025
https://doi.org/10.5194/tc-19-4373-2025-supplement


The Cryosphere Open Access EGU

*Supplement of*

# Damage intensity increases ice mass loss from Thwaites Glacier, Antarctica

**Yanjun Li et al.**

*Correspondence to:* Yanjun Li (liyj375@mail.sysu.edu.cn) and Gang Qiao (qiaogang@tongji.edu.cn)

**Table S1.** Summary of the damage sensitivity experiments and two control experiments performed at the TG basin under constant present-day conditions. The values of parameters $C_1$ and $C_{tr}$ of the 43 simulations considering the damage processes are produced using Latin hypercube sampling in their parameter space. The RMSE and rRMSE between the simulated and observed ice velocity (Rignot et al., 2017) are used to evaluate the accuracy of the model results. The experiments marked with an asterisk* in Group 2 correspond to 18 simulations that predominantly exhibit high damage intensity, leading to model failure before 2300; these simulations are collectively referred to as $G2_{ext}$ in this study.

| Scenarios | ID | Damage parameters | | RMSEs (rRMSEs) over 1990–2020 | | |
|---|---|---|---|---|---|---|
| | | $C_1$ | $C_{tr}$ | RMSE (rRMSE) (whole basin) | RMSE (rRMSE) (floating ice) | RMSE (rRMSE) (grounded ice) |
| Ctrl<br>deactivated damage processes | | – | – | 190.9 (1.58) | 745.2 (0.92) | 95.6 (1.15) |
| $Ctrl_{dhdt}$<br>deactivated damage processes; corrected SMB using satellite-observed ice mass-change rates (Bevan et al., 2023) | | – | – | 181.3 (1.5) | 752.7 (0.97) | 71 (0.84) |
| Group 1<br>damage processes;<br>the contribution to Sea-level (SLC) within the range of observational estimates ± 2 s.d. (0.24 ± 0.08 cm over 1992–2017) in the historical simulation (Shepherd et al., 2019) | 1 | 0.0308 | 0.9861 | 606.6 (5.03) | 2468.7 (3.12) | 77.8 (1.04) |
| | 2 | 0.0576 | 0.7712 | 327.7 (2.72) | 1394.3 (1.68) | 67.1 (0.87) |
| | 3 | 0.0585 | 0.5215 | 221.1 (1.84) | 928.1 (1.12) | 62.5 (0.8) |
| | 4 | 0.0657 | 0.3400 | 196.8 (1.63) | 815 (0.98) | 63.6 (0.81) |
| | 5 | 0.0806 | 0.6590 | 271.4 (2.25) | 1137.4 (1.37) | 65.4 (0.85) |
| | 6 | 0.0838 | 0.5067 | 233 (1.93) | 974.2 (1.16) | 63.4 (0.82) |
| | 7 | 0.0909 | 0.3521 | 194.8 (1.62) | 805.4 (0.97) | 60.4 (0.77) |
| | 8 | 0.0951 | 0.5530 | 249.4 (2.07) | 1041 (1.25) | 63.9 (0.83) |
| | 9 | 0.1014 | 0.3265 | 192.3 (1.6) | 794.2 (0.95) | 60.2 (0.77) |
| | 10 | 0.1297 | 0.3007 | 192.3 (1.6) | 791.1 (0.95) | 59.2 (0.76) |
| | 11 | 0.1385 | 0.4258 | 234.3 (1.95) | 967.1 (1.17) | 62.8 (0.82) |
| | 12 | 0.1399 | 0.2846 | 189.4 (1.57) | 776.2 (0.93) | 59.7 (0.77) |
| | 13 | 0.1780 | 0.2613 | 185.9 (1.54) | 760 (0.91) | 60.2 (0.77) |
| | 14 | 0.1819 | 0.2600 | 185.6 (1.54) | 757.8 (0.91) | 60.3 (0.77) |
| | 15 | 0.1932 | 0.2591 | 185.2 (1.54) | 756.2 (0.91) | 60.2 (0.77) |
| | 16 | 0.2255 | 0.2588 | 184.9 (1.54) | 754.4 (0.91) | 59.9 (0.77) |
| Group 2:<br>damage processes;<br>SLC outside the range of observational estimates ± 2 s.d. in the historical simulation | 1 | 0.0174 | 0.9257 | 178.8 (1.48) | 709.7 (0.88) | 77.6 (0.95) |
| | 2 | 0.0249 | 0.1666 | 181.1 (1.5) | 705.8 (0.87) | 87.3 (1.06) |
| | 3 | 0.0429 | 0.3302 | 193.2 (1.6) | 795.9 (0.96) | 67.3 (0.85) |
| | 4* | 0.0682 | 0.9409 | 560.8 (4.65) | 2217 (2.76) | 106.7 (1.48) |
| | 5 | 0.0778 | 0.1783 | 184.1 (1.53) | 755.1 (0.91) | 64.8 (0.82) |
| | 6* | 0.1232 | 0.9702 | 1092 (9.09) | 3962.9 (5.05) | 260.8 (3.95) |
| | 7* | 0.1381 | 0.8655 | 554.8 (4.59) | 2134.1 (2.66) | 128.5 (1.81) |
| | 8* | 0.1486 | 0.6384 | 489.8 (4.06) | 1980.6 (2.39) | 104.6 (1.44) |
| | 9 | 0.1579 | 0.5134 | 270 (2.24) | 1114.8 (1.35) | 63 (0.83) |

| | | | | | | |
|---|---|---|---|---|---|---|
| | 10* | 0.1759 | 0.8237 | 427.3 (3.52) | 1603 (1.99) | 126.6 (1.79) |
| | 11 | 0.1807 | 0.4473 | 253.3 (2.1) | 1043.6 (1.26) | 63.1 (0.83) |
| | 12* | 0.1911 | 0.6941 | 404.2 (3.34) | 1586.3 (1.94) | 102.6 (1.42) |
| | 13* | 0.2267 | 0.7377 | 403 (3.32) | 1508.7 (1.87) | 123.9 (1.75) |
| | 14 | 0.2335 | 0.3962 | 246.7 (2.05) | 1015 (1.23) | 62.9 (0.83) |
| | 15 | 0.2411 | 0.4244 | 301.7 (2.5) | 1246.1 (1.5) | 67.3 (0.9) |
| | 16* | 0.2604 | 0.467 | 512.1 (4.25) | 2076.9 (2.48) | 112.1 (1.55) |
| | 17 | 0.2812 | 0.3218 | 212.7 (1.77) | 868.6 (1.05) | 62 (0.81) |
| | 18* | 0.3068 | 0.648 | 359.8 (2.97) | 1334.9 (1.64) | 124.1 (1.76) |
| | 19* | 0.3497 | 0.6175 | 552.9 (4.56) | 2057.9 (2.52) | 165.6 (2.39) |
| | 20* | 0.3674 | 0.6608 | 1186.3 (9.73) | 4249.6 (5.27) | 301.6 (4.61) |
| | 21* | 0.3789 | 0.4358 | 526.8 (4.37) | 2140.1 (2.53) | 118.2 (1.63) |
| | 22* | 0.3877 | 0.6057 | 622.4 (5.13) | 2291 (2.8) | 190.8 (2.79) |
| | 23* | 0.4129 | 0.5769 | 574 (4.74) | 2140.6 (2.57) | 183.5 (2.66) |
| | 24* | 0.428 | 0.5242 | 273.4 (2.27) | 1018.8 (1.22) | 109.9 (1.53) |
| | 25* | 0.4538 | 0.5433 | 289.8 (2.4) | 1075.1 (1.29) | 112.1 (1.58) |
| | 26* | 0.4711 | 0.5318 | 262 (2.17) | 983.3 (1.18) | 100.3 (1.4) |
| | 27* | 0.5202 | 0.5657 | 624 (5.15) | 2330.4 (2.81) | 192.7 (2.79) |

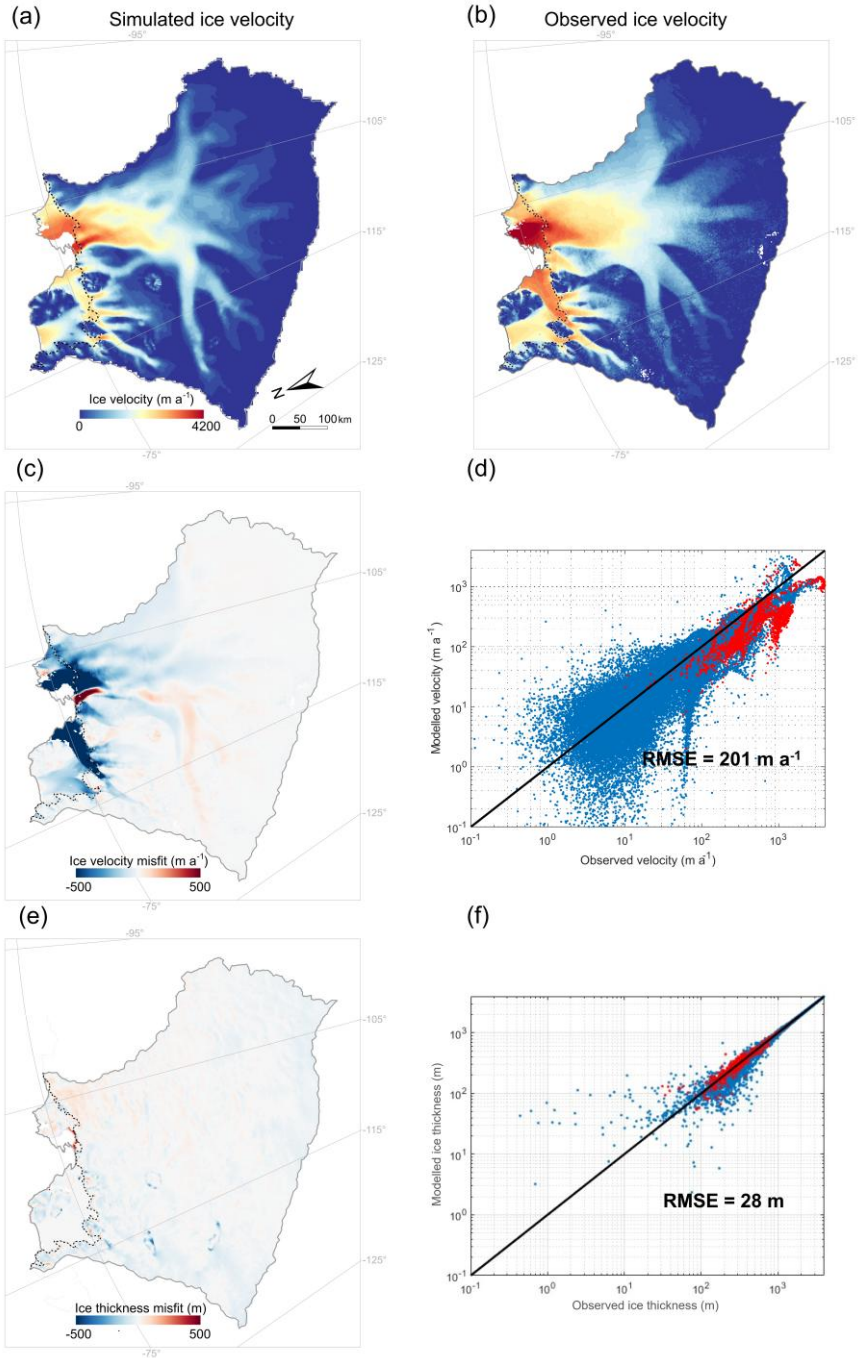


**Figure S1.** Simulated present-day state for the equilibrium initialization obtained with the 1995–2014 atmospheric climatology from MARv3.11 (Kittel et al., 2021). (a) Simulated ice velocity, (b) observed velocity (Rignot et al., 2017), (c) simulated minus observed ice velocity, (d) point-by-point scatter plots of simulated and observed ice-sheet (blue) and ice-shelf (red) velocities, (e) simulated minus observed ice thickness (Morlighem et al., 2020), and (f) point-by-point scatter plots of simulated and observed ice-sheet (blue) and ice-shelf (red) thickness. The dashed black and gray lines are the observed (Gardner et al., 2018) and simulated grounding lines, respectively. The solid light gray line delineates the TG basin boundary based on Zwally et al. (2015).

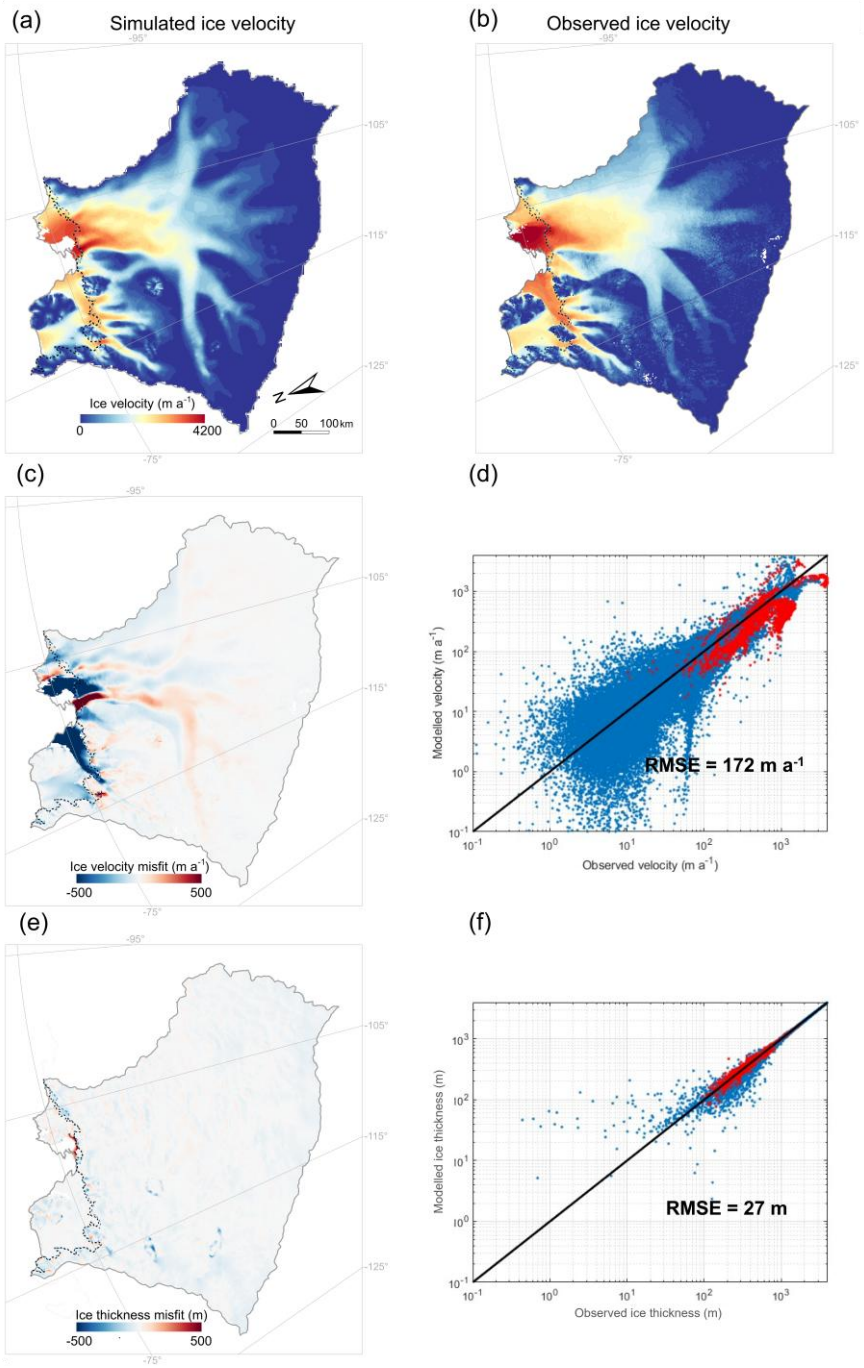


**Figure S2.** Simulated present-day state, same as Figure S1 but with mass balance correction using surface elevation change of the Amundsen Sea Embayment over the period 1992–2019 (Bevan et al., 2023). (a) Simulated ice velocity. (b) observed velocity (Rignot et al., 2017). (c) simulated minus observed ice velocity. (d) point-by-point scatter plots of simulated and observed ice-sheet (blue) and ice-shelf (red) velocities. (e) simulated minus observed ice thickness (Morlighem et al., 2020), and (f) point-by-point scatter plots of simulated and observed ice-sheet (blue) and ice-shelf (red) thickness. The dashed black and blue lines are the observed (Gardner et al., 2018) and simulated grounding lines, respectively. The solid light gray line delineates the TG basin boundary based on Zwally et al. (2015).

**References**


Bevan, S., Cornford, S., Gilbert, L., Otosaka, I., Martin, D., and Surawy-Stepney, T.: Amundsen Sea Embayment ice-sheet mass-loss predictions to 2050 calibrated using observations of velocity and elevation change, Journal of Glaciology, 69(278), 1729-1739, doi:10.1017/jog.2023.57, 2023.

Gardner, A. S., Moholdt, G., Scambos, T., Fahnstock, M., Ligtenberg, S., van den Broeke, M., and Nilsson, J.: Grounding Line for Antarctic Discharge (GLAD) point files for flux estimates, available at: ftp://ftp.nsidc.org/pub/DATASETS/nsidc0732_landsat_antarctic_ice_velocities_v01/GardnerEtAl_2018_ SupData/GLAD_flux_gates/, last access: 9 July 2024, 2018.

Kittel, C., Amory, C., Agosta, C., Jourdain, N. C., Hofer, S., Delhasse, A., Doutreloup, S., Huot, P.-V., Lang, C., Fichefet, T., and Fettweis, X.: Diverging future surface mass balance between the Antarctic ice shelves and grounded ice sheet, The Cryosphere, 15, 1215–1236, doi:10.5194/tc-15-1215-2021, 2021.

Morlighem, M., Rignot, E., Binder, T., Blankenship, D., Drews, R., Eagles, G., Eisen, O., Ferraccioli, F., Forsberg, R., Fretwell, P., Goel, V., Greenbaum, J. S., Gudmundsson, H., Guo, J., Helm, V., Hofstede, C., Howat, I., Humbert, A., Jokat, W., Karlsson, N. B., Lee, W. S., Matsuoka, K., Millan, R., Mouginot, J., Paden, J., Pattyn, F., Roberts, J., Rosier, S., Ruppel, A., Seroussi, H., Smith, E. C., Steinhage, D., Sun, B., van den Broeke, M. R., van Ommen, T. D., van Wessem, M., and Young, D. A.: Deep glacial troughs and stabilizing ridges unveiled beneath the margins of the Antarctic ice sheet, Nature Geoscience, 13(2), 132–137, doi:10.1038/s41561-019-0510-8, 2020.

Rignot, E., Mouginot, J. and Scheuchl, B.: MEaSUREs InSAR-Based Antarctica Ice Velocity Map, Version 2 [Date Accessed]. Boulder, Colorado USA. NASA National Snow and Ice Data Center Distributed Active Archive Center, doi:10.5067/D7GK8F5J8M8R, 2017.

Shepherd, A., Gilbert, L., Muir, A. S., Konrad, H., McMillan, M., Slater, T., Briggs, K. H., Sundal, A. V., Hogg, A. E., and Engdahl, M. E.: Trends in Antarctic Ice Sheet Elevation and Mass, Geophysical Research Letters, 46(14), 8174 – 8183, doi:10.1029/2019GL082182, 2019.

Zwally, H. J., Li, J., Robbins, J. W., Saba, J. L., Yi, D., and Brenner, A. C.: Mass gains of the Antarctic ice sheet exceed losses, Journal of Glaciology, 61(230), 1019–1036, doi:10.3189/2015JoG15J071, 2015.